

# Design of frequency independent optic-axis Pancharatnam based achromatic half-wave plate

Kunimoto Komatsu<sup>a</sup>, Hirokazu Ishino<sup>a</sup>, Nobuhiko Katayama<sup>b</sup>, Tomotake Matsumura<sup>b</sup>, Yuki Sakurai<sup>b</sup>

<sup>a</sup>Department of Physics, Okayama University, Okayama, Japan

<sup>b</sup>Kavli Institute for Physics, Mathematics for Universe (WPI), the University of Tokyo, Chiba, Japan

**Abstract.** Pancharatnam based achromatic half-wave plate (AHWP) achieves high polarization efficiency over broadband. It generally comes with a feature of which the optic-axis of AHWP has dependence of the electromagnetic frequency of the incident radiation. When the AHWP is used to measure the incident polarized radiation with a finite detection bandwidth, this frequency dependence causes an uncertainty in the determination of the polarization angle due to the limited knowledge of a detection band shape and a source spectral shape. To mitigate this problem, we propose new designs of the AHWP that eliminate the frequency dependent optic-axis over the bandwidth and maintain high modulation efficiency. We carried out the optimization by tuning the relative angles among the individual half-wave plates of the five- and nine-layer AHWPs. The optimized set of the relative angles achieves the frequency independent optic-axis over the fractional bandwidth of 1.3 and 1.5 for the five- and nine-layer AHWPs, respectively. We also study the susceptibility of the alignment accuracy to the polarization efficiency and the frequency independent optic-axis, which provides a design guidance for each application.

**Keywords:** Millimeter wave polarimetry, Achromatic half-wave plate, Angle calibration, CMB polarization.

\*Kunimoto Komatsu, [k.komatsu@s.okayama-u.ac.jp](mailto:k.komatsu@s.okayama-u.ac.jp)

## 1 Introduction

The measurement of the cosmic microwave background (CMB) has been playing an important role in the modern cosmology. In recent years, the required sensitivity of CMB polarization telescopes are to probe nano-Kelvin fluctuations on top of 3 K CMB itself. This sensitivity allows to probe the primordial B-mode from the inflationary universe. One of the key requirements for a CMB telescope is to be able to probe the large angular scale, where the inflationary signal is expected. Correspondingly, the instrumental stability is required over the long time scale during its scan and the suppression of the systematics at the large angular scale is essential. A continuously rotating half-wave plate (HWP) can relax some of the stringent requirements. The continuously rotating HWP in an optical path of the telescope modulates the incident polarized signal, and thus we can apply the lock-in technique to the incident polarized signal. As a result, the signal band of the linearly polarized light can be up-converted above the time scale of the system instability. Also, the requirement to avoid any mismatch of the detector properties between detector pairs, e.g. beam, gain, band-pass, can be relaxed. While the HWP can play a crucial role to mitigate the systematic effects in CMB polarimetry, the stringent requirement is also applied to the specification of the HWP itself.

There is no sky area that is free from the Galactic foreground emissions. Therefore, it is essential to observe over broadband and subtract the contributions from the foreground emissions by using the difference of the spectral shapes. A HWP is a birefringent material that is cut to a specific thickness to satisfy the retardance of  $\delta = \pi$ . The frequency that does not satisfy this condition results in the reduction of a conversion efficiency from linear to linear polarization states,

which leads to the degradation of the polarized sensitivity of a polarimeter. A conventional solution to increase the bandwidth is to use a recipe proposed by Pancharatnam, which employs three wave plates stacked together with specific relative angles among them.<sup>1,2</sup> In this paper, we call the multi-layered HWP that follows the Pancharatnam recipe as achromatic HWP (AHWP). Further investigations had addressed the extension of this original work to the five- and nine-layered AHWP.<sup>3-5</sup> A single layer HWP can achieve about 0.4 of the fractional bandwidth for the polarization efficiency of above 0.9, and an AHWP can generally cover the fractional bandwidth of 1.0, 1.3, 1.4, and 1.5 for 3, 5, 7, and 9 layers, respectively.

While the AHWP achieves a broader bandwidth of a polarization efficiency, one caveat is that it introduces a frequency dependence on the effective fast axis of the AHWP. This means that a polarimeter using an AHWP has a frequency dependent polarization angle sensitivity. The other way to phrase is that  $Q$  and  $U$  signals defined in a telescope coordinate is no longer defined by the physical orientation of a polarization sensitive axis, and it varies over the observing electromagnetic frequency. In principle, such this effect can be corrected with a perfect knowledge of a spectral response of an instrument and a source. Any limited knowledge of them can lead to the uncertainty of the polarization angle sensitive orientation. The typical required accuracy of a polarization angle for future inflationary B-mode CMB polarization experiments probing the tensor-to-scalar ratio of  $10^{-3}$  is in the range of  $1 - 10$  arcmin for both absolute and relative angles<sup>6-9</sup> This is a stringent calibration requirement, and it is desirable if we do not have to take into account the additional effect from the frequency dependent optic-axis. In recent years, there are studies to investigate the impact of this effect in the context of the CMB polarization experiment.<sup>10,11</sup> The analysis based mitigation has been also proposed.<sup>12,13</sup> In this paper, we have studies the numerical optimization of the AHWP design to eliminate the spectral dependence of the effective fast optic-axis of an AHWP.

## 2 HWP Polarimetry

### 2.1 Formalism

We present the formalism of HWP polarimetry for our optimization study. Similar descriptions of the formalism can be found in K. Komatsu et al.<sup>5</sup> To simplify a computational step, we ignore the effect of reflection at any surface of a wave plate. The retardance for a single wave plate is defined as

$$\delta(\nu) = 2\pi\nu \frac{d|n_e - n_o|}{c}, \quad (1)$$

where  $\nu$  is the frequency,  $n_o$  and  $n_e$  is the refractive indices for the ordinary and extra-ordinary rays,  $d$  is the thickness of a single wave plate, and  $c$  is the speed of light. The Mueller matrix of the wave plate with the retardance of  $\delta(\nu)$  and the rotation with an angle of  $\chi$  are

$$\gamma(\nu) = \begin{pmatrix} 1 & 0 & 0 & 0 \\ 0 & 1 & 0 & 0 \\ 0 & 0 & \cos \delta(\nu) & -\sin \delta(\nu) \\ 0 & 0 & \sin \delta(\nu) & \cos \delta(\nu) \end{pmatrix}, \quad R(\chi) = \begin{pmatrix} 1 & 0 & 0 & 0 \\ 0 & \cos 2\chi & -\sin 2\chi & 0 \\ 0 & \sin 2\chi & \cos 2\chi & 0 \\ 0 & 0 & 0 & 1 \end{pmatrix}. \quad (2)$$

The  $N$ -layered wave plates with a relative angle  $\chi_i$  for the  $i^{th}$  layer can be written with the rotation matrix  $R$  as

$$\Gamma(\nu) = \prod_i^N R(-\chi_i)\gamma(\nu)R(\chi_i). \quad (3)$$

The Mueller matrix of  $\Gamma$  represents the AHWP. When the incident radiation with the Stokes vector,  $S_{\text{in}}(\nu) = (I_{\text{in}}(\nu), Q_{\text{in}}(\nu), U_{\text{in}}(\nu), V_{\text{in}}(\nu))$  in unit of spectral radiance, propagates through the continuously rotating  $N$ -layered wave plate with an angle  $\rho$ , the output Stokes vector,  $S_{\text{out}}(\nu) = (I_{\text{out}}(\nu), Q_{\text{out}}(\nu), U_{\text{out}}(\nu), V_{\text{out}}(\nu))$ , is written as

$$S_{\text{out}}(\nu) = R(-\rho)\Gamma(\nu)R(\rho)S_{\text{in}}(\nu). \quad (4)$$

The radiation, which passes through the AHWP, is detected by a linearly polarization sensitivity detector. We simplify this step in our modeling by defining a perfect wire grid,  $G$ , along the  $x$ -axis as also shown in Fig. 1, and selecting the intensity component of the final Mueller matrix. As a result, the detected signal can be written as

$$I_{\text{det}}(\nu) = (GS_{\text{out}}(\nu))\Big|_I, \quad (5)$$

where

$$G = \frac{1}{2} \begin{pmatrix} 1 & 1 & 0 & 0 \\ 1 & 1 & 0 & 0 \\ 0 & 0 & 0 & 0 \\ 0 & 0 & 0 & 0 \end{pmatrix}. \quad (6)$$

In this paper, we set  $V_{\text{in}}(\nu) = 0$  by assuming no circularly polarized light in the CMB. The detected intensity  $I_{\text{det}}(\nu)$  as a function of the HWP angle  $\rho$  can be written as

$$\begin{aligned} I_{\text{det}}(\nu) = & D_{0I}(\nu)I_{\text{in}}(\nu) + D_{0Q}(\nu)Q_{\text{in}}(\nu) + D_{0U}(\nu)U_{\text{in}}(\nu) \\ & + D_{2I}(\nu)I_{\text{in}}(\nu)\cos(2\rho - 2\phi_0(\nu)) + D_2(\nu)\sqrt{Q_{\text{in}}(\nu)^2 + U_{\text{in}}(\nu)^2}\cos(2\rho - 2\phi_2(\nu)) \\ & + D_4(\nu)\sqrt{Q_{\text{in}}(\nu)^2 + U_{\text{in}}(\nu)^2}\cos(4\rho - 4\phi_4(\nu)). \end{aligned} \quad (7)$$

The polarization efficiency and the phase are  $2D_4(\nu)$  and  $\phi_4(\nu)$ , respectively. It is worth stressing that these two variables depend on the frequency of the incident radiation for an AHWP while only the polarization efficiency depends on the frequency for a single HWP. Each term in this equation

can be related to the Mueller matrix element of  $\Gamma(\nu)$  as

$$\begin{aligned}
D_{0I}(\nu) &= \frac{1}{2}M_{II}(\nu), \\
D_{0Q}(\nu) &= \frac{1}{4}(M_{QQ}(\nu) + M_{UU}(\nu)), \\
D_{0U}(\nu) &= \frac{1}{4}(M_{QU}(\nu) - M_{UQ}(\nu)), \\
D_{2I}(\nu) &= \frac{1}{2}\sqrt{M_{UI}(\nu)^2 + M_{QI}(\nu)^2}, \\
\phi_0(\nu) &= \frac{1}{2}\arctan \frac{M_{UI}(\nu)}{M_{QI}(\nu)}, \\
D_2(\nu) &= \frac{1}{2}\sqrt{M_{IQ}(\nu)^2 + M_{IU}(\nu)^2}, \\
\phi_2(\nu) &= \frac{1}{2}\arctan \frac{M_{IU}(\nu)}{M_{IQ}(\nu)} + \frac{1}{2}\arctan \frac{U_{in}(\nu)}{Q_{in}(\nu)}, \\
D_4(\nu) &= \frac{1}{4}\sqrt{(M_{QQ}(\nu) - M_{UU}(\nu))^2 + (M_{QU}(\nu) + M_{UQ}(\nu))^2}, \\
\phi_4(\nu) &= \frac{1}{4}\arctan \frac{M_{QU}(\nu) + M_{UQ}(\nu)}{M_{QQ}(\nu) - M_{UU}(\nu)} + \frac{1}{4}\arctan \frac{U_{in}(\nu)}{Q_{in}(\nu)},
\end{aligned} \tag{8}$$

where the element of  $\Gamma(\nu)$  is generalized as

$$\Gamma(\nu) = \begin{pmatrix} M_{II}(\nu) & M_{IQ}(\nu) & M_{IU}(\nu) & M_{IV}(\nu) \\ M_{QI}(\nu) & M_{QQ}(\nu) & M_{QU}(\nu) & M_{QV}(\nu) \\ M_{UI}(\nu) & M_{UQ}(\nu) & M_{UU}(\nu) & M_{UV}(\nu) \\ M_{VI}(\nu) & M_{VQ}(\nu) & M_{VU}(\nu) & M_{VV}(\nu) \end{pmatrix}. \tag{9}$$

To account the finite bandwidth, we integrate the detected intensity over the bandwidth as

$$\langle I_{det} \rangle = \int_0^\infty w(\nu) I_{det}(\nu) d\nu, \tag{10}$$

where  $w(\nu)$  is the weight function to take into account a detailed band shape. If we pick up the final term in Eq. 7, we can write

$$\int_0^\infty w(\nu) D_4(\nu) \sqrt{Q_{in}(\nu)^2 + U_{in}(\nu)^2} \cos(4\rho - 4\phi_4(\nu)) d\nu = A_4 \cos(4\rho - 4\Phi_4). \tag{11}$$

The polarization efficiency and the phase from  $\langle I_{det} \rangle$  relate as  $2A_4$  and  $\Phi_4$ . Therefore, we use  $2A_4$  as the figure-of-merit and use the relative angles of the wave plates,  $\chi_i$ , as optimization variables. The thickness of each plate can be used as another optimization parameter, but we did not find the use in our analysis as described in the later sections.

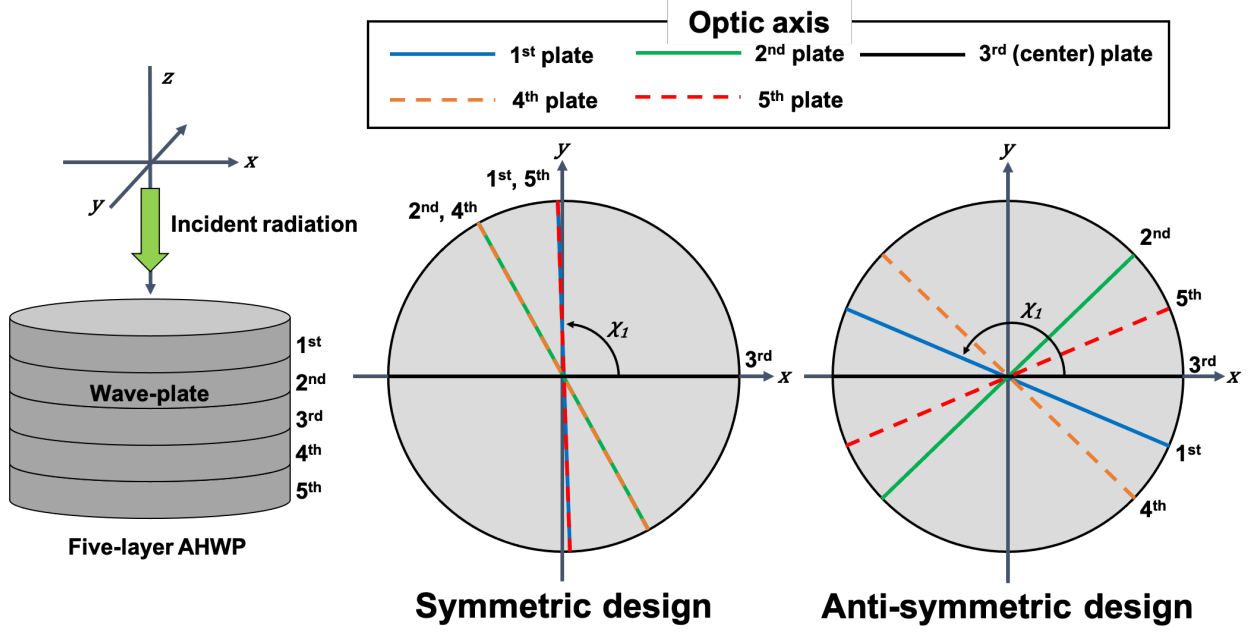


**Fig 1** The conceptual sketch of the symmetric and anti-symmetric designs for the case of a five-layer AHWP.

## 2.2 Optimization

In our optimization, we set the condition for the  $\chi_i$  angle to be oriented in such that each optic-axis angle is anti-symmetric with respect to the angle of the center plate as shown in Fig. 1 to achieve the frequency independent phase. Hereafter, we call this type of AHWP design as “anti-symmetric design”. This condition is the key to realize the frequency-independent optic-axis over the broadband. We use a five-layer anti-symmetric design as an example to describe how the polarization angle rotates through AHWP. In the anti-symmetric design, the first and second plates are rotated with respect to the third plate. The forth and fifth plates are also rotated the same angles with respect to the third plate but the sign of the orientation is opposite from the first and second plates. Namely, we impose the conditions of  $\chi_4 = -\chi_2$  and  $\chi_5 = -\chi_1$  in case of  $N = 5$ . In this way, any offset rotational angle introduced by the first 2.5 plates at each frequency is canceled in the second 2.5 plates. While we achieve the cancellation of the frequency dependent offset angle we still achieve the rotation of the incoming linear polarization plane as the AHWP rotates. The similar concept can be found for the case which two sets of the AHWPs are employed to cancel the frequency dependent effective fast axis response.<sup>14</sup> With this condition, we do not randomize all the  $\chi_i$  angles fully, but randomize only the  $(N - 1)/2$  plates for the  $N$ -layer AHWP.

In the followings, we demonstrate the optimization of the AHWP design by using this anti-symmetric constraint with a specific observational frequency range. LiteBIRD is one of the example projects to apply our AHWP designs. A LiteBIRD low-frequency telescope has the largest frequency coverage, 34-161 GHz, within a single telescope with a presence of a HWP to date,<sup>15</sup> and thus we use this range in our study as an example. We assume a top-hat band shape in this frequency range. In a real application, we should be able to derive the optimized recipe by taking into account the detailed band shape, but this is beyond the scope of this paper. In this work, we assume to use sapphire as a wave plate. The set of the parameters used in this design work is

**Table 1** A summary of the parameters used for the optimization process.

Frequency range, $\nu$	34 – 161 GHz
Center frequency, $\nu_0$	97.5 GHz
Refractive indices, $(n_o, n_e)$	(3.047, 3.361) <sup>16</sup>
Thickness of each plate, $d$	4.9 mm
Incident angle	0 degrees

summarized in Tab. 1.

In the calculation in the optimization, the integration of Eq. 11 is replaced by the summation of Eq. 7 with the frequency resolution of 1 GHz. We calculate  $A_4$  a total of 50,000 times with random distribution of  $\chi_i$  between 0 and 180 degrees for  $S_{in} = (1, 0, 1, 0)$  and find the optimal designs for 3, 5, 7, 9 of layers. The final result does not depend on the detailed choice of  $Q_{in}$  and  $U_{in}$  except the offset of  $\phi_4$ . From this calculation, we choose a set of  $\chi_i$  angles that provide the largest  $A_4$  over the given frequency range.

We have only explored the case with the odd number of the wave plates because of the existing broadband AHWP designs from the past studies.<sup>3,5,17,18</sup> It is worth pointing out that these existing designs tend to have the relative angles to be oriented in symmetric with respect to the angle of the center plate. In order to contrast the results from our anti-symmetric design to the existing designs, we also compute the case in which the optic-axis angles are forced to be set in symmetric with respect to the angle of the center plate as Fig. 1. Hereafter, we call this type of AHWP design as “symmetric design”.

### 3 Results

Tab. 2 and 3 show the results of the parameter searches. We list the fractional bandwidth,  $\Delta\nu/\nu_0$ , that is the ratio of the frequency range with polarization efficiency  $2A_4$  greater than 0.9 to the center frequency of 97.5 GHz. The polarization efficiency is computed within the frequency range in Tab. 1. Fig. 2 shows the polarization efficiency and the phase  $\phi_4$  as a function of the frequency based on the designs listed in Tab. 2 and 3 for  $S_{in} = (1, 0, 1, 0)$ . The cases for the symmetric angle show a broad coverage of the polarization efficiency and the non-flat phase response over the frequency. On the other hand, the anti-symmetric design for  $N = 5$  and 9 can completely eliminate the phase variation over frequency while the polarization efficiency is maintained to be broad.

The quoted bandwidth of the polarization efficiency in Tab. 2 and 3 should be treated as a representative value. Depending on an application, one might allow to have some oscillatory features around the polarization efficiency close to 1 as the  $N = 5$  anti-symmetric design in Fig 2. In this case, there is a possibility that we obtain the broader bandwidth by trading with the degradation of the overall averaged efficiency. In such case, we can increase the bandwidth further. This point is addressed in Sec. 4.2.

We also computed for the three and seven anti-symmetric angles. For  $N = 3$ , we found the solution to be  $\chi_i = (90.00, 0.00, -90.00)$  degrees, which is essentially the same as a single HWP. For  $N = 7$ , we found the solution to be  $\chi_i = (111.73, 43.70, 97.20, 0.00, -97.20, -43.70, -111.73)$  degrees but the calculated polarization efficiency and fractional bandwidth are nearly the same as  $N = 5$ . Therefore, we omit to show in the table and figure due to the redundancy.

The solutions which we have shown in this paper are not unique. For example with the angle set for anti-symmetric ( $N = 5$ ), the same performance can be obtained by the angle set of

$$\chi_1 = 22.67 \pm 180 \times j \quad (12)$$

$$\chi_2 = 133.63 \pm 180 \times j \quad (13)$$

$$\chi_3 = 0.00 \pm 180 \times j \quad (14)$$

$$\chi_4 = -133.63 \pm 180 \times j \quad (15)$$

$$\chi_5 = -22.67 \pm 180 \times j \quad (16)$$

in unit of degrees, where  $j$  is an arbitrary integer because of the spin-2 nature of the wave plate. Therefore, the set of angles may look different but multiple combinations of angles can produce the same performance. Needless to say, there are overall rotational degree of freedom, thus any global rotation, i.e.  $\chi_3 \neq 0$ , added to all the angles  $\chi_i$  still provides the same spectral performance except the change of the global phase offset,  $\phi_4$ .

**Table 2** A summary of anti-symmetric designs

The number of layers $N$	Pol. eff. $2A_4$	Frac. bandwidth $\Delta\nu/\nu_0$	Optic-axis angles $\chi_i$ [deg.]
5	0.978	1.23	22.67 , 133.63 , 0.00 , -133.63 , -22.67
9	0.993	1.35	23.19 , 170.88 , 89.85 , 143.85 , 0.00 , -143.85 , -89.85 , -170.88 , -23.19

**Table 3** Table of symmetric designs

The number of layers $N$	Pol. eff. $2A_4$	Frac. bandwidth $\Delta\nu/\nu_0$	Optic-axis angles $\chi_i$ [deg.]
3	0.894	1.00	58.35 , 0.00 , 58.35
5	0.965	1.33	88.65 , 61.68 , 0.00 , 61.68 , 88.65
7	0.989	1.32	49.76 , 99.86 , 23.20 , 0.00 , 23.20 , 99.86 , 49.76
9	0.993	1.42	1.83 , 66.92 , 15.36 , 132.66 , 0.00 , 132.66 , 15.36 , 66.92 , 1.83

## 4 Discussions

### 4.1 Tolerance analysis

#### 4.1.1 Optic-axis angle alignment

LiteBIRD plans to use the five-layers AHWP. Therefore, as an example, we discuss the alignment tolerances. Fig. 3 shows the relation between the alignment accuracy of  $\chi_i$  and the AHWP performances, the polarization efficiency and the phase, in the case of the  $N = 5$  anti-symmetric design.



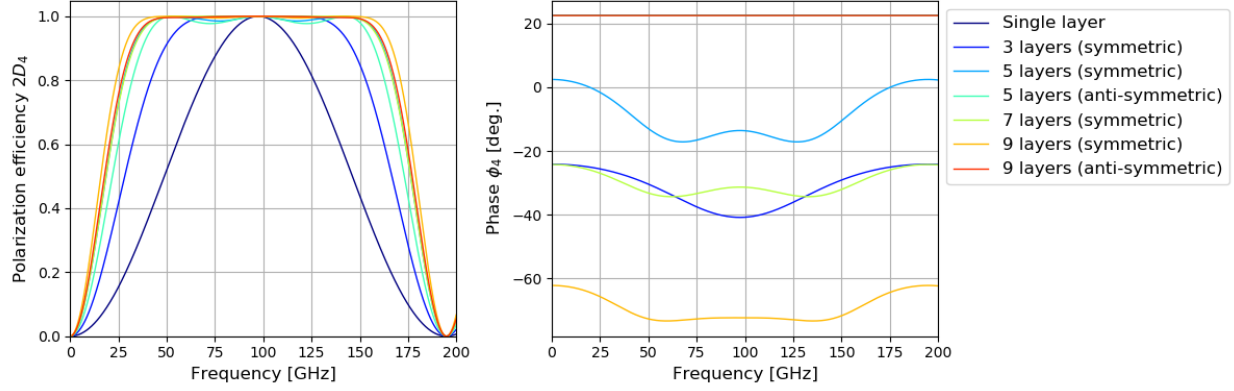


**Fig 2** The comparison of the polarization efficiency and the phase of each design.

We fix all the parameters except the relative HWP angles,  $\chi_i$ , which are randomized with flat distribution for each plate in the range of 1, 5, 10, 15, 20, 30 and 60 arcmin centered at the nominal designed angles. For each case, we compute the polarization efficiency and the phase. We perform this calculation 10,000 times in each case to obtain the range of the performances. Fig. 3 shows the susceptibility to the frequency dependence of the effective fast axis, phase  $\phi_4$ , from the alignment accuracy of each optic-axis angle. To suppress the maximum deviation of the frequency dependent phase to be less than 1 degree, the alignment accuracy of the optic-axis angle is required to be less than 15 arcmin.

#### 4.1.2 Wave plate thickness

We also perform the tolerance analysis to the accuracy of the wave plate thickness. Fig. 4 shows the polarization efficiency and the phase when we add the flat distribution of the random thickness within the range of 5, 10, 20, 30, 50, and 100  $\mu\text{m}$  to the nominal thickness for the  $N = 5$  anti-symmetric design. Each plate thickness is varied independently without any correlation among the plates. We assume that the plates are always adjacent to each other without any gap. From

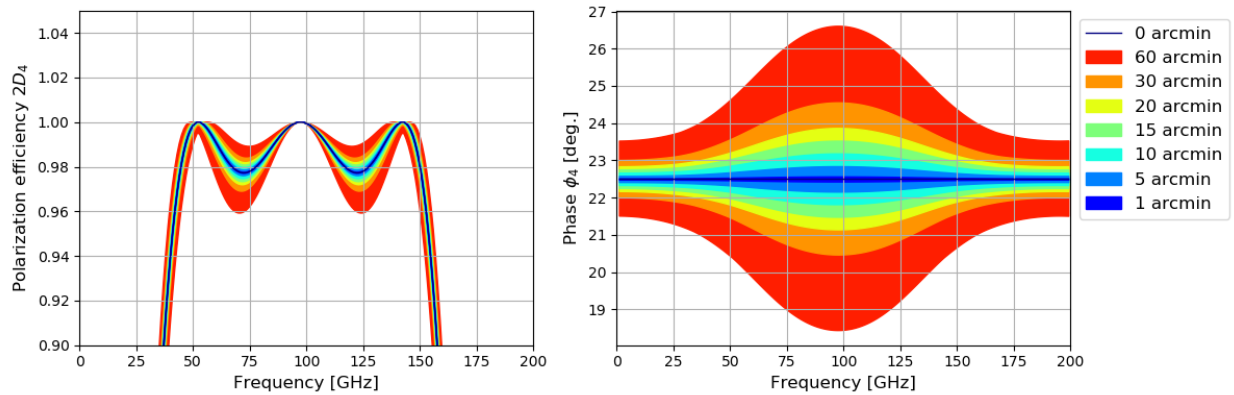


**Fig 3** The relation between the alignment accuracy of the optic-axis angles of each plate and the phase for the  $N = 5$  anti-symmetric design. The left panel shows the polarization efficiency and the right panel shows the phase.



these figures, we identify that the impact is prominent at the higher side of the frequency range. The reason is simply because the higher frequency is more susceptible to the small change of the thickness in order to maintain the same retardance as shown in Eq. 1. The similar impact appears to the phase. At 195 GHz, the retardance with the nominal thickness is  $2\pi$ , and thus  $A_4 = 0$ . Correspondingly, no phase can be defined. The impact of the uncertainty to the phase is also propagated from the last equation in Eq. 8 because the element of the Mueller matrix  $\Gamma$  is a function of the retardance. In order to minimize the maximum phase variation in the frequency range from 34 to 161 GHz to be less than 1 degree, the thickness variation has to be controlled to be less than  $20 \mu\text{m}$ .

#### 4.2 Further optimization for broader frequency coverage

When we allow to have a oscillatory feature near the polarization efficiency of 1, we can broaden the bandwidth as described in Sec. 3. On the other hand, when we do not allow to have a oscilla-

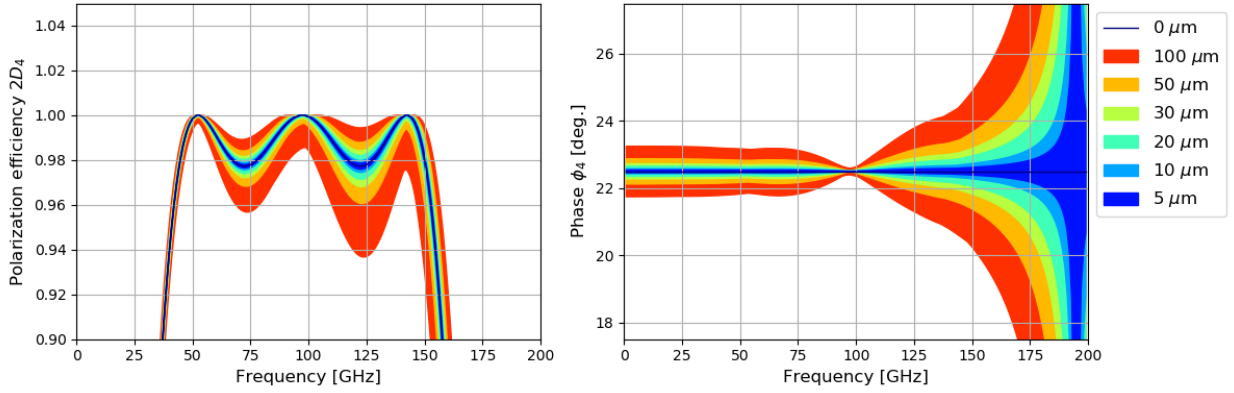


**Fig 4** The relation between the variation of each wave plate thickness and the AHWP performance in the case of the anti-symmetric design five-layer AHWP.

**Table 4** Table of the  $N = 5$  anti-symmetric designs optimized with the various frequency ranges.

Optimization freq. range $\Delta\nu_{opt}$ [GHz]	Optimization bandwidth $\Delta\nu_{opt}/\nu_0$	Polarization efficiency $2A_4$	Fractional bandwidth $\Delta\nu/\nu_0$	Optic-axis angles $\chi_i$ [deg.]
84 – 111	0.28	1.000	1.02	23.28 , 128.13 , 0.00 , -128.13 , -23.28
74 – 121	0.48	1.000	1.04	157.34 , 51.92 , 0.00 , -51.92 , -157.34
64 – 131	0.69	1.000	1.09	23.11 , 129.59 , 0.00 , -129.59 , -23.11
54 – 141	0.89	0.998	1.12	23.55 , 130.70 , 0.00 , -130.70 , -23.55
44 – 151	1.10	0.993	1.17	156.95 , 48.05 , 0.00 , -48.05 , -156.95
34 – 161	1.30	0.978	1.23	22.67 , 133.63 , 0.00 , -133.63 , -22.67
24 – 171	1.51	0.945	1.28	157.83 , 45.21 , 0.00 , -45.21 , -157.83
14 – 181	1.71	0.886	1.31	157.98 , 44.07 , 0.00 , -44.07 , -157.98
4 – 191	1.92	0.806	1.33	21.51 , 136.51 , 0.00 , -136.51 , -21.51

tory feature near the polarization efficiency of 1, the available bandwidth becomes narrower. As test cases, we set the varieties of the frequency range to be optimized. Specifically, we start the frequency range of 34-161 GHz and add/subtract 10 GHz to widen/narrow the bandwidth. We perform the optimizations with nine frequency ranges for the  $N = 5$  and 9 anti-symmetric design. Tab. 4 and 5 show the results from the optimization for each frequency range. We define the optimization fractional bandwidth as  $\Delta\nu_{opt}/\nu_0$ , which is the ratio of the targeted optimization range,  $\Delta\nu_{opt}$ , to the center frequency of 97.5 GHz. Fig. 5 shows the polarization efficiency, phase, and the band averaged polarization efficiency over the optimization bandwidth for all the cases of  $N = 5$ . From the top-left panel of Fig. 5, we confirm that the optimized design has larger oscillatory features at around the polarization efficiency close to 1 when we use broader bandwidth to be optimized. An AHWP designer has to take into account the trade-off between the broad-band availability and the overall averaged polarization efficiency based on each application. This consideration applies the same for both the symmetric and anti-symmetric designs.

#### 4.3 Further design optimization with larger degree of freedoms

The optimizations were carried about by assuming the fixed thickness of each wave plate and by imposing the anti-symmetric condition so far. Here, we do not enforce these conditions. As a result, we take the thickness of all the wave plates and all the relative angles as the free parameters and carry out the optimization with the figure-of-metric of  $2A_4$  for the frequency range of 34-161 GHz. We choose for  $N = 9$ , which gives  $8 + 9$  extra free parameters. Because of this large number of free parameters, we use minuit<sup>19</sup> to maximize  $A_4$  after randomizing the parameters for the optimization in this section. Tab. 6 shows the results of the optimization. All the thicknesses ended up converging to essentially the same value. Fig. 6 shows the polarization efficiency and the

**Table 5** Table of the  $N = 9$  anti-symmetric designs optimized with the various frequency ranges.

Optimization freq. range $\nu_{opt}$ [GHz]	Optimization bandwidth $\Delta\nu_{opt}/\nu_0$	Polarization efficiency $2A_4$	Fractional bandwidth $\Delta\nu/\nu_0$	Optic-axis angles $\chi_i$ [deg.]
84 – 111	0.28	1.000	0.96	11.71 , 154.96 , 56.67 , 66.41 , 0.00 , -66.41 , -56.67 , -154.96 , -11.71
74 – 121	0.48	1.000	1.07	50.10 , 142.71 , 19.65 , 124.47 , 0.00 , -124.47 , -19.65 , -142.71 , -50.10
64 – 131	0.69	1.000	1.08	145.87 , 52.56 , 17.93 , 122.93 , 0.00 , -122.93 , -17.93 , -52.56 , -145.87
54 – 141	0.89	0.999	1.21	0.73 , 139.90 , 42.67 , 60.88 , 0.00 , -60.88 , -42.67 , -139.90 , -0.73
44 – 151	1.10	0.998	1.35	23.19 , 170.88 , 89.85 , 143.85 , 0.00 , -143.85 , -89.85 , -170.88 , -23.19
34 – 161	1.30	0.993		
24 – 171	1.51	0.984	1.50	158.36 , 166.52 , 65.73 , 35.57 , 0.00 , -35.57 , -65.73 , -166.52 , -158.36
14 – 181	1.71	0.957	1.55	20.64 , 4.72 , 108.96 , 150.26 , 0.00 , -150.26 , -108.96 , -4.72 , -20.64
4 – 191	1.92	0.886		

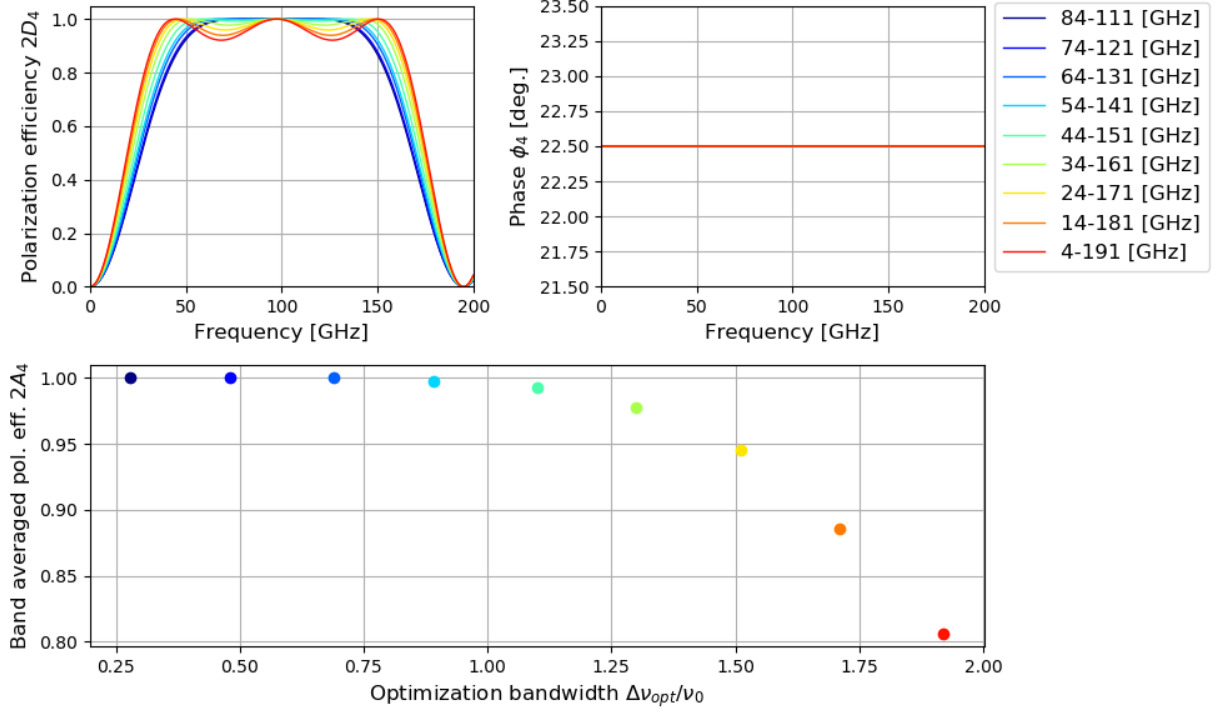


**Fig 5** The comparison of the polarization efficiency and the effective fast axis angle of Tab. 4. The horizontal axis of the bottom plot is the ratio of the optimization frequency range to the center frequency. In the phase plot, the all lines are overlap since the all design have same value.

phase as a function of the frequency with the parameters in Tab. 6 and the case with the thickness being fixed at 4.7 mm. While we thought adding free parameters increase the degree of freedom to find the broader polarization efficiency with a flat phase response but we did not find the broader coverage within the range of our parameter searches. Due to the large number of the free parameters, there may be a room for improvement in the optimization process, but such a investigation is beyond the scope of this paper. However, one of the designs shown in Tab. 6 has the maximum phase variation of about 0.2 degrees over the targeted frequency range without imposing the anti-symmetric condition. This means the anti-symmetric condition is not the only way to reach the flat phase response when we have the large number of the free parameters.

**Table 6** Table of the another design has the smaller frequency dependent optic-axis

The number of layers $N$	Pol. eff. $2A_4$	Frac. bandwidth $\Delta\nu/\nu_0$		
9	0.998	1.48	$\chi_i$ [deg.]	-69.92, 5.13, -7.27, 44.90, 0.00, 109.89, -18.27, -36.60, 29.83
			$d_i$ [mm]	4.694, 4.649, 4.755, 4.686, 4.747, 4.700, 4.743, 4.663, 4.713

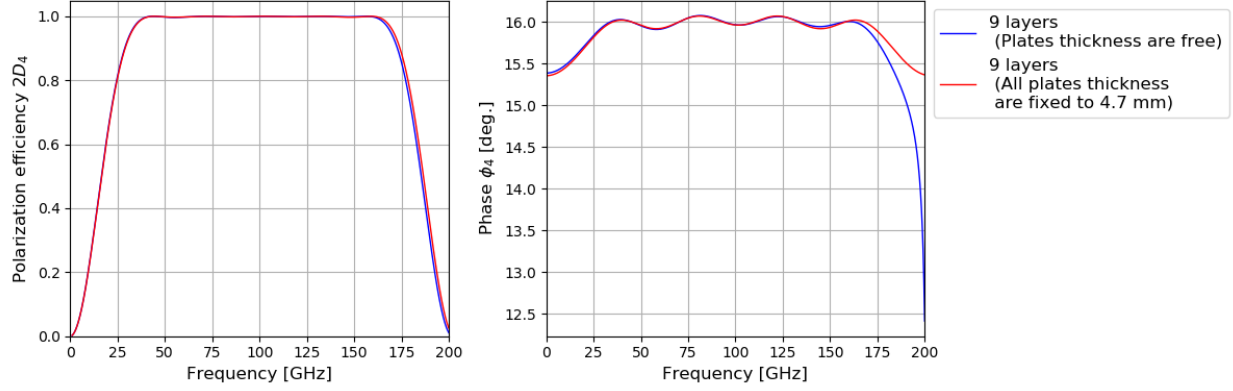


**Fig 6** The polarization efficiency and the effective fast axis angle of the design in Tab. 6.

## 5 Conclusions

A HWP for CMB polarization experiments is in need to cover broadband in order to achieve high sensitivity for the CMB radiation as well as the foreground emissions in a single polarimeter. While an AHWP can broaden the bandwidth, the frequency dependent fast axis of the AHWP can add the challenge in calibration and add the complexity in the analysis. We propose to eliminate this effect with a specific angle set of a novel AHWP by imposing the anti-symmetric orientation to the relative wave plate angles. We derived the examples of the wave plate relative angles for  $N = 5, 9$ . The optimized set of the relative angles achieves the frequency independent optic-axis and covers the fractional bandwidth of 1.3 and 1.5 for five- and nine-layer AHWPs, respectively. We also discussed the tolerance of the design in the wave plate relative angles and thicknesses. In order to minimize the maximum variation of the phase response over the frequency, we need to assemble the AHWP within the relative angles of 15 arcmin and the accuracy of the thickness less than  $20 \mu\text{m}$ . This result can be applicable not limited to the CMB polarimetry but any other applications that require a flat spectral response of the effective fast axis of the AHWP.

## Acknowledgments

This paper based on a SPIE conference proceedings paper.<sup>20</sup> This work was supported by JPSP KAKENHI Grant Number JP17H01125, JP18J20148, JP19K14732, by World Premier International Research Center Initiative (WPI), MEXT, and by the JSPS Core-to-Core program, A. Advanced Research Networks.

## References

- 1 S. Pancharatnam, “Achromatic combinations of birefringent plates part i. an achromatic circular polarizer,” *Proc. of Indian Acad. Sci.-Sect. A* **41**, 130–136 (1955).
- 2 S. Pancharatnam, “Achromatic combinations of birefringent plates part ii. an achromatic quarter-wave plate,” *Proc. of Indian Acad. Sci.-Sect. A* **41**, 137–144 (1955).
- 3 G. Savini *et al.*, “Achromatic half-wave plate for submillimeter instruments in cosmic microwave background astronomy: modeling and simulation,” *Applied Optics* **45**, 8907–8915 (2006).

- 4 T. Matsumura *et al.*, “Analysis of performance of three- and five-stack achromatic half-wave plates at millimeter wavelengths,” *Applied Optics* **48**, 3614–3625 (2009).
- 5 K. Komatsu, T. Matsumura, H. Imada, *et al.*, “Demonstration of the broadband half-wave plate using the nine-layer sapphire for the cosmic microwave background polarization experiment,” *Journal of Astronomical Telescopes, Instruments, and Systems* **5**(4), 1 – 14 (2019).
- 6 Y. Sakurai, T. Matsumura, N. Katayama, *et al.*, “Breadboard model of the polarization modulator unit based on a continuously rotating half-wave plate for the low-frequency telescope of the LiteBIRD space mission,” in *Millimeter, Submillimeter, and Far-Infrared Detectors and Instrumentation for Astronomy X*, J. Zmuidzinas and J.-R. Gao, Eds., **11453**, 743 – 762, International Society for Optics and Photonics, SPIE (2020).
- 7 F. Columbro, P. de Bernardis, L. Lamagna, *et al.*, “A polarization modulator unit for the mid- and high-frequency telescopes of the LiteBIRD mission,” in *Space Telescopes and Instrumentation 2020: Optical, Infrared, and Millimeter Wave*, M. Lystrup, M. D. Perrin, N. Batalha, *et al.*, Eds., **11443**, 1113 – 1128, International Society for Optics and Photonics, SPIE (2020).
- 8 C. A. Hill *et al.*, “Design and development of an ambient-temperature continuously-rotating achromatic half-wave plate for cmb polarization modulation on the polarbear-2 experiment,” in *Millimeter, Submillimeter, and Far-Infrared Detectors and Instrumentation for Astronomy VIII, Proc. SPIE* **9914**(99142U) (2016).
- 9 S. A. Bryan, S. M. Simon, M. Gerbino, *et al.*, “Development of calibration strategies for the Simons Observatory,” in *Millimeter, Submillimeter, and Far-Infrared Detectors and Instrumentation for Astronomy IX*, J. Zmuidzinas and J.-R. Gao, Eds., **10708**, 685 – 697, International Society for Optics and Photonics, SPIE (2018).
- 10 C. Bao, B. Gold, C. Baccigalupi, *et al.*, “The impact of the spectral response of an achromatic half-wave plate on the measurement of the cosmic microwave background polarization,” *The Astrophysical Journal* **747**, 97 (2012).
- 11 C. Bao, C. Baccigalupi, B. Gold, *et al.*, “MAXIMUM LIKELIHOOD FOREGROUND CLEANING FOR COSMIC MICROWAVE BACKGROUND POLARIMETERS IN THE PRESENCE OF SYSTEMATIC EFFECTS,” *The Astrophysical Journal* **819**, 12 (2016).
- 12 M. H. Abitbol, D. Alonso, S. M. Simon, *et al.*, “The simons observatory: Bandpass and polarization-angle calibration requirements for b-mode searches.” <https://arxiv.org/abs/2011.02449> (2020).
- 13 C. Vergès, J. Errard, and R. Stompor, “Framework for analysis of next generation, polarised cmb data sets in the presence of galactic foregrounds and systematic effects.” <https://arxiv.org/abs/2009.07814> (2020).
- 14 T. Matsumura, “Mitigation of the spectral dependent polarization angle response for achromatic half-wave plate.” <https://arxiv.org/abs/1404.5795> (2014).
- 15 M. Hazumi, P. A. Ade, A. Adler, *et al.*, “LiteBIRD satellite: JAXA’s new strategic L-class mission for all-sky surveys of cosmic microwave background polarization,” in *Space Telescopes and Instrumentation 2020: Optical, Infrared, and Millimeter Wave*, M. Lystrup, M. D. Perrin, N. Batalha, *et al.*, Eds., **11443**, International Society for Optics and Photonics, SPIE (2020).
- 16 B. R. Johnson, *MAXIPOL: A Bolometric, Balloon-Borne Experiment for Measuring the Polarization Anisotropy of the Cosmic Microwave Background Radiation*. Ph.d. thesis, University of Minnesota, Twin Cities (2004).

- 17 S. Hanany *et al.*, “Millimeter-wave achromatic half-wave plate,” *Applied Optics* **44**, 4666–4670 (2005).
- 18 G. Pisano *et al.*, “Achromatic half-wave plate for submillimeter instruments in cosmic microwave background astronomy: experimental characterization,” *Applied Optics* **45**, 6982–6989 (2006).
- 19 “imimuit.” <https://iminuit.readthedocs.io/en/stable/>.
- 20 K. Komatsu, H. Ishino, N. Katayama, *et al.*, “Design of the frequency independent optic axis of the Pancharatnam base achromatic half-wave plate for CMB polarization experiment,” in *Millimeter, Submillimeter, and Far-Infrared Detectors and Instrumentation for Astronomy X*, J. Zmuidzinas and J.-R. Gao, Eds., **11453**, 750 – 760, International Society for Optics and Photonics, SPIE (2020).

**First Author** is a PhD student at Okayama University. He received his BS and MS degrees in physics from Okayama University in 2016 and 2018, respectively. His current research interests the verification of inflation theory using B-mode polarization of CMB created by the primordial gravitational waves. Related to it, he is developing the polarization modulator of LiteBIRD.

## List of Figures

- 1 The conceptual sketch of the symmetric and anti-symmetric designs for the case of a five-layer AHWP.
- 2 The comparison of the polarization efficiency and the phase of each design.
- 3 The relation between the alignment accuracy of the optic-axis angles of each plate and the phase for the  $N = 5$  anti-symmetric design. The left panel shows the polarization efficiency and the right panel shows the phase.
- 4 The relation between the variation of each wave plate thickness and the AHWP performance in the case of the anti-symmetric design five-layer AHWP.
- 5 The comparison of the polarization efficiency and the effective fast axis angle of Tab. 4. The horizontal axis of the bottom plot is the ratio of the optimization frequency range to the center frequency. In the phase plot, the all lines are overlap since the all design have same value.
- 6 The polarization efficiency and the effective fast axis angle of the design in Tab. 6.

## List of Tables

- 1 A summary of the parameters used for the optimization process.
- 2 A summary of anti-symmetric designs
- 3 Table of symmetric designs
- 4 Table of the  $N = 5$  anti-symmetric designs optimized with the various frequency ranges.
- 5 Table of the  $N = 9$  anti-symmetric designs optimized with the various frequency ranges.
- 6 Table of the another design has the smaller frequency dependent optic-axis